Global Simulation of Magnetospheric Space Weather Effects of the Bastille Day Storm

J. Raeder and Y. L. Wang
Institute of Geophysics and Planetary Physics, University of California, Los Angeles

T. J. Fuller-Rowell and H. J. Singer
NOAA Space Environment Center, Boulder, Colorado

Abstract. We present results from a global simulation of the interaction of the solar wind with Earth's magnetosphere, ionosphere, and thermosphere for the Bastille Day geomagnetic storm and compare the results with data. We find that during this event the magnetosphere becomes extremely compressed and eroded, causing 3 geosynchronous GOES satellites to enter the magnetosheath for an extended time period. At its extreme, the magnetopause moves at local noon as close as $4.9R_E$ to Earth which is interpreted as the consequence of the combined action of enhanced dynamic pressure and strong dayside reconnection due to the strong southward interplanetary magnetic field component B_z, which at one time reaches a value of -60nT. The lobes bulge sunward and shield the dayside reconnection region, thereby limiting the reconnection rate and thus the cross polar cap potential. Modeled ground magnetic perturbations are compared with data from 37 sub-auroral, auroral, and polar cap magnetometer stations. While the model can not yet predict the perturbations and fluctuations at individual ground stations, its predictions of the fluctuation spectrum in the 0-3 mHz range for the sub-auroral and high-latitude regions are remarkably good. However, at auroral latitudes (63° to 70° magnetic latitude) the predicted fluctuations are slightly too high.

1. Introduction

Contemporary terrestrial weather forecasts rely on a combination of dense observation networks and sophisticated numerical models which project the current weather conditions into the future. Similarly, space weather forecasting will require large scale numerical models of Earth's space environment as a key operational element, along with sufficient timely observations to provide model input and to initialize model fields. Besides their utility for space weather forecasting, such models are also essential tools to understand the environment and the plasma physical processes in it, because *in situ* measurements are often too sparse to enable a unique interpretation of the data, and because the complexity of the space environment limits our theoretical understanding. By comparing predictions with data, large scale models also serve to test our knowledge about the prevailing processes, i.e., successful model predictions suggest that the assumptions underlying the model are correct, whereas model failures point to deficiencies of our understanding. Models have also become an increasingly important tools to analyze and interpret experimental data, by putting *in situ* measurements from a single (or at most a few) spacecraft into perspective and thus extending the "view" of the observations. Thus, progress is often made by combining data analysis with global modeling, since both are essentially complementary. In the foreseeable future tens to hundreds of spacecraft might provide data, in which case models will also play a crucial role in assimilating these measurements in order to provide global synoptic maps of Earth's space environment.

No global comprehensive model of Earth's space environment exists today. However, regional models have been developed that treat limited regions or processes. For example, global MHD models cover the outer magnetosphere (Ogino, 1986; Tanaka, 1995; Janhunen et al., 1995; Lyon et al., 1998; Winglee and Menietti, 1998; Gombosi et al., 1998; Raeder, 1999), but omit the particle drift physics of the inner magnetosphere within a few R_E from Earth as well as the plasma and neutral constituents of the ionosphere–thermosphere system. Some of these models (Fedder and Lyon, 1987; Tanaka, 1995; Janhunen et al., 1995; Lyon et al., 1998; Raeder, 1999; Raeder et al., 2000; Raeder et al., 2001a; Raeder et al., 2001b) include an ionosphere submodel that solves a potential equation to close the field aligned currents originating in the magnetosphere. The ionospheric conductance in these submodels is either taken to be

constant or derived by using empirical models for EUV ionization and parameterizations for electron precipitation in the auroral zone (Slinker et al., 1998; Raeder, 1999). However, such submodels do not fully represent the ionosphere–thermosphere system, but approximate only one aspect of it, namely the closure of field aligned currents, and rely on a number of approximations and parameterizations.

On the other hand, fully dynamical models of the ionosphere–thermosphere system exist, for example the Thermosphere Ionosphere Mesosphere Electrodynamics General Circulation Model (TIME-GCM) (Roble and Ridley, 1994) or the NOAA Coupled Thermosphere Ionosphere Model (CTIM) (Fuller-Rowell et al., 1996). These models depend on magnetospheric input, for example the electric field and particle precipitation. For the lack of direct observations of these quantities with sufficient resolution, they are usually taken from empirical (climatological) models, parameterizations, or data-assimilative models, for example AMIE (Richmond and Kamide, 1988).

Clearly, comprehensive models of Earth's space environment require the coupling of magnetosphere models with ionosphere–thermosphere models because these types of models are complementary. The global magnetosphere models lack the physical first-principle calculations at the ionospheric end which can be provided by an ionosphere–thermosphere (IT) model; vice versa, IT models require input that magnetosphere models can provide, and at the same time provide input to magnetosphere models. We have recently coupled the UCLA magnetosphere-ionosphere (MI) model with the NOAA thermosphere-ionosphere model (CTIM) and presented first results from a simulation of the January 10/11, 1997 geomagnetic storm (Raeder et al., 2001b). We found that the coupled model significantly improves the predicticted ground magnetometer response, which was attributed to the much more realistic ionospheric conductances that CTIM self-consistently provides. In this paper we expand on this work with a simulation study of the Bastille Day (July 14-16, 2001) storm, which has so far been one of the largest geomagnetic storms of this solar cycle. We show that our model correctly predicts the erosion of the magnetosphere and the entry of three geosynchronous GOES spacecraft into the magnetosheath. We also show the detailed response of modeled ground magnetometers and compare them with data. Each of these predictions is of importance for space weather, because geosynchronous spacecraft entering the magnetosheath are often disrupted in their operations, and strong ground magnetic perturbations cause ground induced currents that can interrupt power systems and cause pipeline corrosion.

2. The Model

The model that is used in this study has already been discussed in the literature, thus we give only a brief description here. Specifically, the UCLA MI model is described in Raeder (1999) and Raeder et al. (2001a); CTIM is discussed by Fuller-Rowell et al. (1996) and the coupled model is introduced in Raeder et al. (2001b).

Briefly, the UCLA global MI model solves the MHD equations in a large volume surrounding Earth such that the entire interaction region between the solar wind and the magnetosphere is included. Specifically, the simulation domain comprises the bow shock, the magnetopause, and the magnetotail up to several hundred R_E from Earth. Thus the model input is given by the solar wind plasma and IMF (Interplanetary Magnetic Field), which usually comes from measurements of a solar wind monitoring satellite. This model has been developed and continually improved over the many years and now goes well beyond a "three-dimensional global MHD simulation model." Besides numerically solving the MHD equations with high spatial resolution, the model also includes ionospheric processes and their electrodynamic coupling with the magnetosphere. The coupling between the magnetosphere and the ionosphere is an essential part of the model because the ionosphere controls to a large part magnetospheric convection, by providing the resistive closure of the field aligned currents that are generated from the interaction of the solar wind with the magnetosphere (Raeder et al., 1998). Processes that occur in the near-Earth region

on polar cap and auroral field lines and that are inherently kinetic have been parameterized in the model using empirical relationships (Raeder et al., 2001a). These processes include the field aligned potential drops that are associated with upward field aligned currents and related electron precipitation, and the diffuse electron precipitation that is caused by pitch angle scattering of plasma sheet electrons (Lyons et al., 1979; Kennel and Petschek, 1966; Weimer et al., 1987). These electron precipitation parameters are then used as input for CTIM. In turn, the MI model uses the conductances and the field aligned currents to solve the ionospheric potential equation. The embedded ionosphere model yields many ionospheric quantities that are observable from the ground and low Earth orbiting satellites, including the field aligned currents, the Hall and Pedersen conductances, the electric potential, the total and the equivalent ionospheric current, the dissipation rates, and ground magnetic perturbations. In particular, the ground magnetic perturbation can be computed at any point of the auroral zone and the polar cap, as well as related geomagnetic indices like the AE, AU, and AL indices. The availability of the synthetic magnetograms and indices allows for direct comparisons with ground data (Raeder et al., 2001a).

The CTIM part of the coupled model is a global multi-fluid model of the thermosphere–ionosphere system with a long heritage (Fuller-Rowell et al., 1996). CTIM solves both neutral and ion fluid equations self-consistently from 80 to 500 km for the neutral atmosphere and from 80 to 10,000 km for the ionosphere on a spherical grid with 2° latitude resolution and 18° longitude resolution. The thermosphere part solves the continuity equation, horizontal momentum equation, energy equation, and composition equations for the major species O, O_2, and N_2 on 15 pressure levels. The ionosphere model part solves the continuity equations, ion temperature equation, vertical diffusion equations, and horizontal transport for H^+ and O^+, while chemical equilibrium is assumed for N_2^+, O_2^+, NO^+, and N^+. The horizontal ion motion is governed by the magnetospheric electric field. The coupled model includes about 30 different chemical and photo-chemical reactions between the species. CTIM's primary inputs are the solar UV and EUV fluxes (parameterized by the solar 10.7 cm radio flux), the tidal modes (forcing from below), auroral precipitation, and the magnetospheric electric field, each of which is usually taken from parameterized empirical models. CTIM provides several outputs that are of prime importance for space weather, for example global two- and three-dimensional ionosphere and thermosphere state fields, like electron density, neutral density, neutral wind, chemical composition, NmF2, hmF2, and total electron content (TEC). A more thorough description of CTIM, including the detailed equations, reaction rates, and examples can be found in (Fuller-Rowell et al., 1996).

In coupling the MI model with CTIM, the MI model provides the electron precipitation parameters and the magnetospheric electric field. In turn, CTIM provides the ionospheric conductance and the ionospheric dynamo current to the MI model. Thus, as far as the MI model is concerned, we replace empirical conductance calculations (Robinson et al., 1987) that was used in most prior studies with first-principle calculations and also account for the ionospheric dynamo effect. The latter effect is probably of minor importance in most situations, but may become significant during storm recovery (Richmond and Roble, 1987). With this coupling, CTIM is also driven with more realistic magnetospheric inputs and depends on fewer empirical parameters.

3. Solar Wind and Interplanetary Magnetic Field

Figure 1 shows the most important solar wind and IMF parameters for this event. The IMF parameters are from the ACE magnetometer and the plasma data have been recovered and compiled from Wind-SWE data that were originally contaminated by the solar proton event associated with this storm (courtesy of Al Lazarus and Justin Kasper, MIT). The top two panels of Figure 1 show the IMF B_y and B_z components, followed by the solar wind speed, the number density, the magnetosonic Mach number, and the plasma β (ratio of the plasma pressure to the magnetic pressure). An interplanetary shock arrives at $\sim$1430 UT

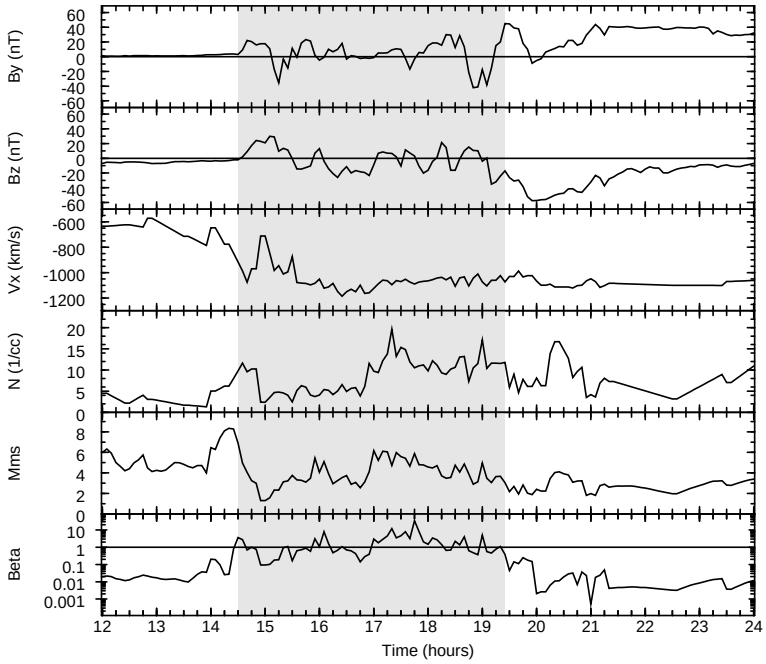

Figure 1. Solar wind and IMF measurements for July 15, 2000. From top to bottom: The IMF B_y and B_z components, the solar wind velocity, the solar wind number density, the solar wind magnetosonic Mach number, and the plasma β (ratio of plasma pressure to magnetic field pressure). The shaded region is the CME sheath, which begins at the interplanetary shock and ends with the CME proper, which is defined here as the magnetic flux rope.

and initiates the event. The plasma density and the magnetic field increase, as well as the solar wind speed, which eventually reaches values of up to 1200 km s^{-1}. The passage of the sheath of this Coronal Mass Ejection (CME) lasts for several hours until ∼1910 UT, when the CME proper arrives. The CME sheath is characterized by increased magnetic field, velocity, and density. The IMF B_z fluctuates strongly and reaches values of ∼-20 nT several times. As the CME proper arrives, the IMF B_z turns strongly southward and reaches a minumum of -60 nT at ∼2000 UT. Such extreme values of B_z are rarely seen in the solar wind, and lead, as we will show in the following, to severe erosion of the magnetosphere. B_z stays southward for several more hours and slowly recovers to smaller values. At the same time the plasma beta is very low ($\sim 10^{-2}$) and the solar wind Mach number is also unusually low (∼2).

The solar wind and IMF data presented in Figure 1 were used as input to the global simulation. In addition, the IMF B_x and the transverse solar wind flow components were set to zero. Using the IMF B_x as input is generally difficult (see: Raeder et al., 2001a for a discussion), and the transverse flows are of little consequence for the magnetospheric response. Neglecting the IMF B_x component has also only a minor influence, as long as it is not the dominant field component.

4. Magnetospheric Compression and Erosion

The increase of the solar wind dynamic pressure associated with the initial interplanetary shock is expected to compress the magnetosphere. In addition, the southward component of the IMF reconnects with the magnetospheric field at the dayside magnetopause, leading to the erosion of the magnetosphere on the dayside. Either of these effects is generally not sufficient to bring the magnetopause, which is usually located ∼10 R_E from Earth, to within geosynchronous distance (∼6.6 R_E). The effects of this

storm on the magnetosphere are more severe because both the solar wind dynamic pressure is strong, and the IMF B_z is strongly southward at times as well.

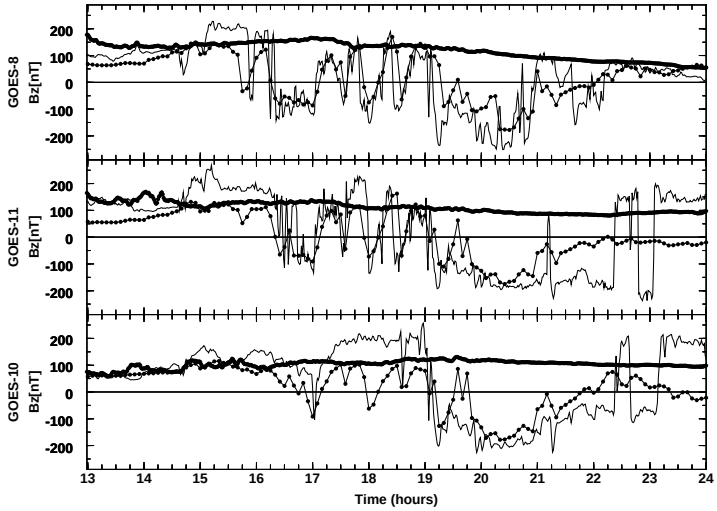

Figure 2. The magnetic field component B_z observed by the 3 GOES satellites (from top to bottom: GOES 8, GOES 11, and GOES 10, ordered in increasing east longitude). The GOES data on July 15, 2000 are plotted as black solid lines, the corresponding model results as black lines with dots, and the GOES data for July 13, 2000 are plotted as thick black line. The latter data are from a typical geomagnetically quiet day.

Figure 2 shows the B_z component (in GSE, that is, Geocentric Solar Ecliptic, coordinates) measured by three geosynchronous GOES satellites (GOES 8 at 285.3° east longitude, GOES 10 at 224.8° east longitude, and GOES 11 at 255.7° east longitude). The thick black lines show the field 2 days prior to the event (July 13, 2000), which was a typical quiet day. The thin black lines show the GOES data on July 15, 2000, and the thin black lines with dots show the results from the simulation. As expected, the field exhibits essentially only a small diurnal variation during the quiet day. On July 15, the field becomes initially compressed around 1500 UT when the interplanetary (IP) shock impacts the magnetosphere and the solar wind dynamic pressure increases. This effect is most noticeable, starting at ∼1437 UT, at GOES 8 and GOES 11 that are closest to the dayside at this time. At ∼1550 UT the field at GOES 8 becomes briefly negative, indicating that GOES 8 enters the magnetosheath. At this time GOES 8 is located at 1040 magnetic local time (MLT), while GOES 10 is located at 0655 MLT and GOES 11 at 0840 MLT. GOES 11 enters the magnetosheath next, at 1615 UT (0910 MLT), and GOES 10 at 1700 UT (0752 MLT). Subsequently, all three GOES spacecraft exit and re-enter the magnetosheath multiple times during the passage of the CME sheath. However, with the arrival of the CME proper at ∼1920 UT all 3 spacecraft enter the magnetosheath for an extended period, lasting for about 3 hours. This extended magnetosheath excursion is due to the fact that all 3 spacecraft pass through local noon around this period (GOES 8 at ∼1705 UT, GOES 10 at ∼2052 UT, and GOES 11 at ∼1854 UT).

The dotted lines (simulation results) follow the GOES data extremely well. The simulation essentially predicts all of the magnetopause crossings, with the exception of very few, mostly at the end of the interval. From this we can conclude that the principal physical processes, in particular the rate of magnetic reconnection, the magnetopause pressure balance, and the control of magnetospheric convection by the ionosphere are modeled correctly. While each of these processes has been addressed in previous studies, it has been far from clear whether the model would be able to predict the magnetopause location for an extreme event such as this storm. While it may appear to be overkill to use a complex model like ours to

predict the magnetopause location, it is also true that empirical models are most likely unable to make such predictions because the solar wind and IMF parameters of this event are well outside the range of validity for empirical models.

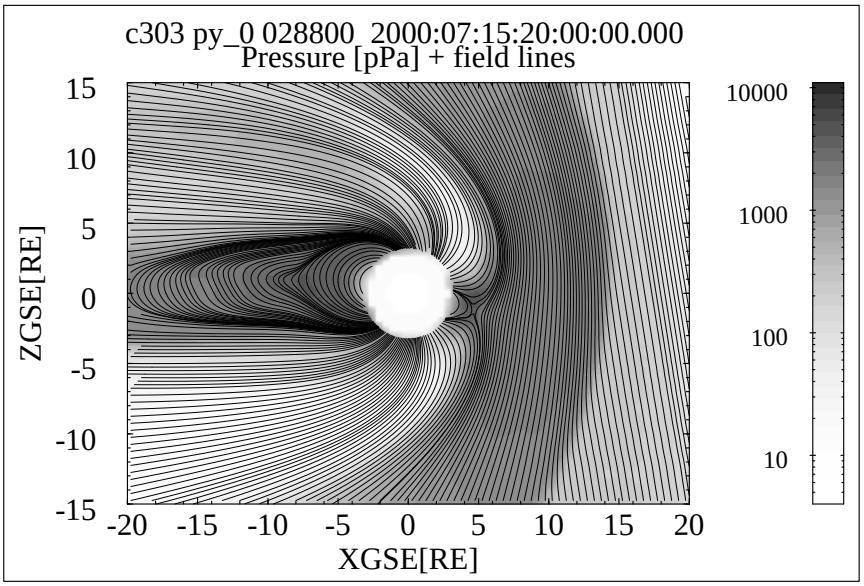

Figure 3. Cut of the noon-midnight meridional plane shows the plasma pressure in grayscale and magnetic field lines at 2000 UT on July 15, 2000.

Figure 3 shows a cut in the noon-midnight meridian with the plasma pressure and magnetic field lines around the time when the dayside magnetosphere is most eroded (2000 UT). The magnetopause, as defined by the last closed field line, is at this time located $4.9R_E$ from Earth at local noon. The topology of the dayside magnetosphere is very unusual. While the dipolar region is shrunk and of very limited extent in latitude, the lobes bulge out sunward. Thus, much of the magnetic flux that is removed from the magnetosphere cannot readily convect to the nightside. As a consequence, the cusp and the polar cap move sunward and to low latitudes. This topology makes the magnetosphere a more blunt object as compared to times of more benign solar wind conditions. The standoff distance of the bow shock therefore remains comparatively large, which is also a consequence of the low magnetosonic Mach number of the solar wind (see Figure 1). The bulging of the lobes apparently shields the magnetopause reconnection region to some extent from the compressed IMF in the magnetosheath. In order to reach the magnetopause, the plasma and field has to penetrate the region between the outbulging lobes, which is a stagnation region with very small flow velocities that limits the convection of the IMF towards the reconnection site. It appears that the magnetosphere regulates magnetopause reconnection by this process, and consequently also the cross polar cap potential, which in this simulation rarely exceeds 300 kV. If the potential scaled linearly with the southward IMF B_z component, the potential would reach values of $\sim$1000 kV. Thus, this type of shielding of the magnetopause reconnection region may explain the saturation of the cross polar cap potential that has been observed in earlier studies (Weimer et al., 1990; Russell et al., 2001).

The dynamics of this event can be viewed in greater detail in the animation that accompanies this paper (note to the editor: how do we cite and refer to the animation?). The animation shows a three-dimensional rendering of the magnetosphere. First, the camera moves around the magnetosphere to show the magnetospheric structures from all sides. After that, the magnetosphere time evolution is shown from a fixed location (0900 MLT, 15° elevation in GSE coordinates). The noon-midnight meridional plane

shows color coded the plasma pressure (purple and blue: low values, green: intermediate values, yellow and red: high values), and the plane at Z_{GSE}=-3R_E shows the plasma velocity with the same color scale. The black arrows indicate the velocity; they are scaled to the square root of the velocity magnitude. A pink field line is anchored at (20,0,0) R_E in the solar wind, along with a red arrow that shows the IMF direction and magnitude (this arrow disappears when the IMF is small). The 3 GOES satellites (from west to east: GOES 10, GOES 11, and GOES 8) are marked by small spheres, along with the field lines passing through them. A set of blue-colored field lines is traced from 65° magnetic latitude every 5° in longitude. The blue sphere at the center of the coordinate system is the inner boundary of the MHD simulation and has a radius of 3.5R_E.

The animation starts before the IP shock hits the magnetosphere. At this time the IMF is northward and the magnetosphere is in a quiet state. As the IP shock hits, the magnetosphere becomes compressed; however, not as much as to put the GOES satellites into the magnetosheath. As the IMF turns southward the magnetosphere becomes quickly eroded and subsequently the GOES spacecraft enter the magnetosheath. While the CME sheath passes over the magnetosphere several episodes of northward and southward IMF occur, alternately placing the GOES spacecraft into the magnetosheath and back into the magnetosphere. At ∼1930 UT the CME sheath proper arrives with a prolonged interval of southward IMF, causing extreme erosion of the magnetosphere. The IMF then slowly rotates back to a northward direction at ∼0200 UT on July 16, leading to the re-closure of the previously open blue field lines, that is, the polar cap retreats poleward.

5. Ionospheric and Ground Magnetic Effects

An important aspect of space weather are the ground perturbations that are caused by the magnetosphere-ionosphere coupling and the resulting currents in the ionosphere (also called “electrojets”). In Figure 4 we compare the north-south component of the modeled ground perturbation with data from a number of ground magnetometers. The modeled perturbations are calculated from first-principles, that is, using Biot-Savart’s law (see Raeder et al. (2001a) for details). Figure 4 shows in the left column the comparison of the north-south ground magnetic perturbation at 8 different sites, ordered from north to south, and at 1 min time resolution. The data are drawn in black lines, and the model results are drawn in red lines. There is generally a reasonable agreement between the data and the model results. In particular, the overall magnitudes of the ground perturbations are reasonably well represented. However, at times the model misses intensifications, and at other times the model predicts intensifications that do not occur. Besides the 8 stations shown here, we have compared the model results with data from 30 other ground magnetometers, all of which are located in the northern polar cap, the auroral zone, or the sub-auroral zone. We find that the model results generally agree better with the observations in the polar cap, on the dayside, and at most sub-auroral stations. Stations with the largest discrepancies tend to be located in the auroral zone and on the nightside.

The right column of Figure 4 shows the time derivative of the ground magnetic perturbation for the corresponding stations of the left column. This quantity is generally of more importance for practical space weather forecasting because it is directly related to the induced electric field and thus to ground induced currents (GICs) that affect power transmission systems and pipelines. Because taking the derivative magnifies the differences between the model and the data we expect a worse correlation compared to the comparison of the magnetic field values. This is indeed the case. Although there is certainly no one to one correlation between the individual peaks of the data and the simulation results, the amplitudes of the fluctuations are comparable for many of these stations. Because $\partial\mathbf{B}/\partial t$ is characterized by short term fluctuations it makes thus more sense to compare the spectral charateristics of these time series.

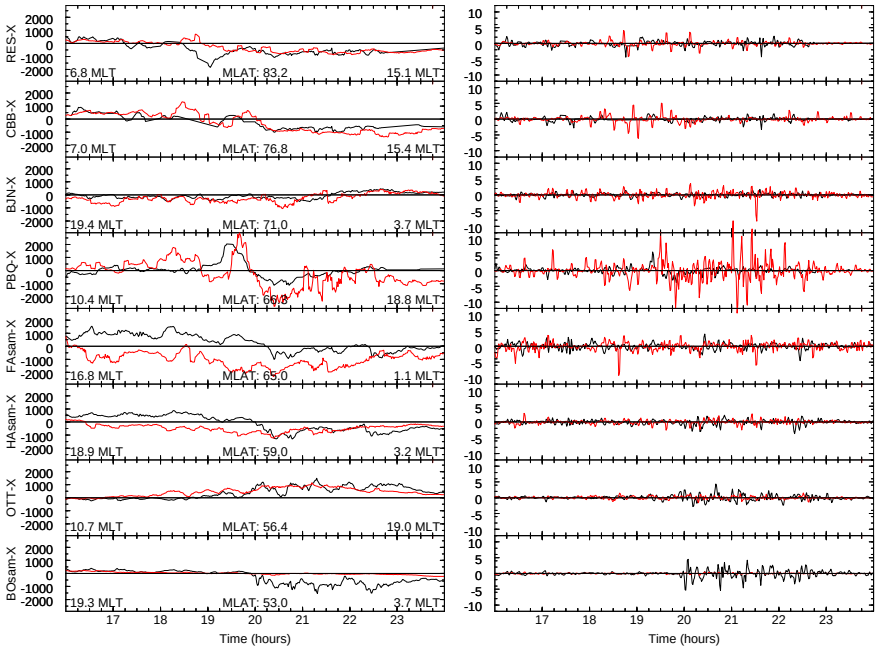

Figure 4. The north-south ground magnetic perturbation (left column, the scale is in nT) and the corresponding time derivative (right column, the scale is in nT/s) for 8 ground magnetometer stations. The station names are indicated at the left of each panel, and the stations are ordered from north to south, although at different magnetic local times. Specifically, these stations are, with their abbreviation, geographic longitude and latitude given in parentheses: Resolute Bay (RES, 74.7°, 265.2°), Cambridge Bay (CBB, 69.1°, 255.0°), Bear Island (BJN, 74.52°, 19.02°), Poste-d.l.-Baleine (PBQ, 55.3°, 282.3°), Faroes (FAsam, 62.1°, 353.0°), Hankasalmi (HAsam, 62.3°, 26.7°), Ottawa (OTT, 45.4°, 284.5°), and Borok (BOsam, 58.0°, 38.3°).

Figure 5 shows the averaged power spectral density (PSD) of the north-south field perturbation for 37 ground magnetometer stations in the polar cap, the auroral, and the sub-auroral regions of the northern hemisphere. Included in these averages are 16 sub-auroral stations ($<63°$ magnetic latitude), 18 auroral stations (between 63° and 70° magnetic latitude), and 7 high-latitude polar cap stations (above 70° magnetic latitude). In spite of the significant differences at individual stations between the model predictions and the actual observations, the average PSD of the modeled ground magnetometers compares very well with the observed one, in particular in the 0-3 mHz range in the sub-auroral zone and at high latitudes. This is true for both the field perturbations and the time derivative of the field perturbation. Above 3 mHz and up to the Nyquist frequency of the 1 min data used here (8.3 mHz) the model overestimates the PSD, but at most by a factor of 2.

It is at this point not clear what causes the particular fluctuation levels. Part of it may just be due to fluctuations in the solar wind and the IMF that propagate through the magnetosphere and ionosphere. However, judging from the dynamics at individual stations this should only be a minor contribution because the fluctuations at different stations do not seem to be strongly correlated, neither in the observations, nor in the model. Thus, the largest part of the fluctuations must derive from the internal dynamics of the magnetosphere.

6. Discussion and Summary

We have used the UCLA/NOAA coupled magnetosphere-ionosphere-thermosphere model to simulate the magnetospheric and ionospheric effects of the Bastille day storm. Of the multitude of variables that the

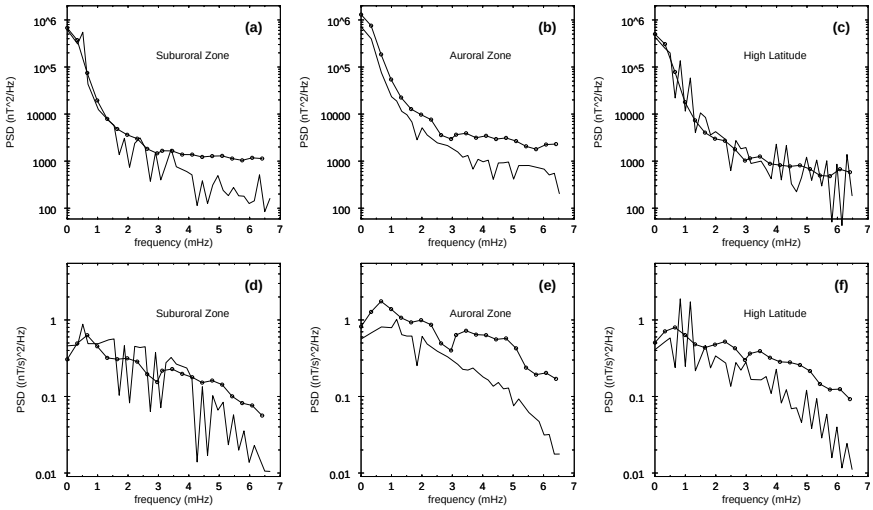

Figure 5. (a-c) shows the averaged power spectral density (PSD, in units of nT^2Hz^{-1}) of the north-south perturbation for ground magnetometer stations in the sub-auroral zone (a), the auroral zone (b), and the polar cap (c). The solid line is for the data, the solid line with dots represents the model result. The lower panel (d-f) shows the average PSD of the time derivative of the north-south perturbation (in units of $nT^2s^{-2}Hz^{-1}$) for the same set of stations.

model provides, we discuss the compression and erosion of the magnetosphere and the ground magnetic perturbations in detail because of their relevance for space weather applications. Our main findings are:

1. The Bastille day storm causes an extreme compression and erosion of the magnetosphere. The magnetopause comes as close as $4.9R_E$ (geocentric) to Earth, causing three geosynchronous satellites that are separated by almost 4 hours in local time to enter the magnetosheath almost simultaneously for about three hours. Thus, the sector of the geosynchronous orbit that lies outside the magnetopause is at least 4 hours, and possibly as much as 7 hours wide.

2. As a consequence of the magnetopause erosion the lobes bulge out sunward and the magnetospheric cusps move equatorward. This effect partly shields the dayside reconnection region from the magnetosheath flow and field. The dayside reconnection rate is therefore reduced, leading to the limitation (and possibly saturation, this will be addressed in a forthcoming paper) of the cross polar cap potential. The shielding also prevents the magnetopause from moving even further inward.

3. The modeled ground magnetic perturbations in the northern hemisphere polar cap, auroral, and subauroral region compare reasonably well with the observations. As we found in a previous study (Raeder et al., 2001a) the magnitude of the electrojets is modeled fairly well; however, the location of the electrojets may be off by several degrees. Since a ground magnetometer senses ionospheric current at most 100 km away, these displacements lead to relatively poor correlation between the measured and the modeled ground pertubations at individual stations. The results of this paper are consistent with this picture because the modeled averaged magnetic field fluctuation are in much better agreement with the observations in spite of the fact that large discrepancies exist at the individual magnetometers.

4. The averaged fluctuation spectrum over 38 ground magnetometers is very well modeled, in particular in the 0-3 mHz range. The spectrum seems not to be due to fluctuations in the solar wind and IMF, but rather due to the internal dynamics of the magnetosphere. This allows us to conclude that the model captures the internal dynamics of the magnetosphere rather well, in spite of the rather crude

MHD description. This result is in line with our recent finding that substoms can be modeled with some accuracy (Raeder et al., 2001a), including the highly variable magnetic reconnection in the tail with the associated spatially bounded fast flow episodes. The latter are likely responsible for the fluctuations of the ionospheric currents because of the intimate links between the magnetosphere and the ionosphere.

As a final note we would like to point out that these simulations were run in better than real-time on 64 nodes of the IBM-SP2 at the San Diego Supercomputer Center. Thus, with a reliable and continuous solar wind and IMF data stream, real-time operational space weather forecasts would be possible with a model like ours. However, the experience with the Wind plasma instrument, which was blinded by the solar proton event associated with this storm, also shows the importance of developing and using instruments "immune" to severe space weather effects for space weather operations.

Acknowledgements

We would like to thank Justin Kasper and the MIT Space Plasma Group for providing us the Wind plasma data. Level 2 ACE magnetometer data were provided by the JPL ACE website. Ground magnetometer data from the Geophysical Institute Magnetometer Array (Dr. J. Olson), the UK Sub-Auroral Magnetometer Network (The authors thank Dr. I. R. Mann and Dr. D. K. Milling for the SAMNET data. SAMNET is a PPARC National Facility deployed and operated by the University of York, UK.), and from the IMAGE (International Monitor for Auroral Geomagnetic Effects) magnetometer chain were used. The IMAGE magnetometer data are collected as a Finnish - German - Norwegian - Polish - Russian - Swedish project. The work at UCLA was supported by grants ATM-0097143 and ATM-0084483 from the National Science Foundation. Computations were performed on the IBM-SP2 of the San Diego Supercomputer Center and the SGI-Origin2000 at the National Center for Supercomputer Applications.

References

Fedder, J. A. and J. G. Lyon: 1987, 'The Solar wind - magnetosphere - ionosphere current - voltage relationship'. *Geophys. Res. Lett.* **14**, 880.

Fuller-Rowell, T. J., D. Rees, S. Quegan, R. J. Moffett, M. V. Codrescu, and G. H. Millward: 1996, 'A coupled thermosphere-ionosphere model (CTIM)'. In: R. W. Schunk (ed.): *STEP Report*. NOAA/NGDC, Boulder, Colorado, p. 217, Scientific Committee on Solar Terrestrial Physics (SCOSTEP).

Gombosi, T. I., D. L. DeZeeuw, C. P. T. Groth, K. G. Powell, and P. Song: 1998, 'The length of the magnetotail for northward IMF: Results of 3D MHD simulations'. In: T. Chang and J. R. Jasperse (eds.): *Phys. Space Plasmas (1998)*, Vol. 15. Cambridge, Mass.: p. 121.

Janhunen, P., T. I. Pulkkinen, and K. Kauristie: 1995, 'Auroral fading in ionosphere-magnetosphere coupling model: Implications for possible mechanisms'. *Geophys. Res. Lett.* **22**, 2049.

Kennel, C. F. and H. E. Petschek: 1966, 'Limit on Stably Trapped Particle Fluxes'. *J. Geophys. Res.* **71**, 1.

Lyon, J. G., R. E. Lopez, C. C. Goodrich, M. Wiltberger, and K. Papadopoulos: 1998, 'Simulation of the March 9, 1995, substorm: Auroral brightening and the onset of lobe reconnection'. *Geophys. Res. Lett.* **25**, 3039.

Lyons, L. R., D. Evans, and R. Lundin: 1979, 'An Observed Relation Between Magnetic Field Aligned Electric Fields and Downward Electron Energy Fluxes in the Vicinity of Auroral Forms'. *J. Geophys. Res.* **84**, 457.

Ogino, T.: 1986, 'A three dimensional MHD simulation of the interaction of the solar wind with the Earth's magnetosphere: The generation of field aligned currents'. *J. Geophys. Res.* **91**, 6791.

Raeder, J.: 1999, 'Modeling the magnetosphere for northward interplanetary magnetic field: Effects of electrical resistivity'. *J. Geophys. Res.* **104**, 17357.

Raeder, J., J. Berchem, and M. Ashour-Abdalla: 1998, 'The Geospace Environment Modeling Grand Challenge: Results from a Global Geospace Circulation Model'. *J. Geophys. Res.* **103**, 14787.

Raeder, J., R. L. McPherron, L. A. Frank, W. R. Paterson, J. B. Sigwarth, G. Lu, H. J. Singer, S. Kokubun, T. Mukai, and J. A. Slavin: 2001a, 'Global simulation of the Geospace environment modeling substorm challenge event'. *J. Geophys. Res.* **106**, 381.

Raeder, J., O. Vaisberg, V. Smirnov, and L. Avanov: 2000, 'Reconnection driven lobe convection: Interball tail probe observations and global simulations'. *J. Atm. Solar-Terr. Phys.* **62**, 833.

Raeder, J., Y. Wang, and T. Fuller-Rowell: 2001b, 'Geomagnetic storm simulation with a coupled magnetosphere-ionosphere-thermosphere model'. In: P. Song, G. Siscoe, and H. J. Singer (eds.): *Space Weather, AGU Geophys. Monogr. Ser.* p. in press, American Geophysical Union.

Richmond, A. D. and Y. Kamide: 1988, 'Mapping Electrodynamic Features of the High Latitude Ionosphere from Localized Observations'. *J. Geophys. Res.* **93**, 5741.

Richmond, A. D. and R. G. Roble: 1987, 'Electrodynamic effects of thermospheric winds for the NCAR thermospheric general circulation model'. *J. Geophys. Res.* **92**, 12365.

Robinson, R. M., R. R. Vondrak, K. Miller, T. Dabbs, and D. Hardy: 1987, 'On Calculating Ionospheric Conductances from the Flux and Energy of Precipitating Electrons'. *J. Geophys. Res.* **92**, 2565.

Roble, R. G. and E. C. Ridley: 1994, 'A Thermosphere - Ionosphere - Mesosphere - Electrodynamics General Circulation Model (TIME-GCM): Equinox solar cycle minimum simulations (30-500 km)'. *Geophys. Res. Lett.* **21**, 417.

Russell, C. T., J. G. Luhmann, and G. Lu: 2001, 'Nonlinear response of the polar ionosphere to large values of the interplanetary electric field'. *J. Geophys. Res.* **in press**.

Slinker, S. P., J. A. Fedder, J. Chen, and J. G. Lyon: 1998, 'Global MHD simulation of the magnetosphere and ionosphere for 1930-2330 UT on November 3, 1993'. *J. Geophys. Res.* **103**, 26243.

Tanaka, T.: 1995, 'Generation mechanisms for magnetosphere-ionosphere current systems deduced from a three-dimensional MHD simulation of the solar wind-magnetosphere-ionosphere coupling processes'. *J. Geophys. Res.* **100**, 12057.

Weimer, D. R., D. A. Gurnett, C. K. Goertz, J. D. Menietti, J. L. Burch, and M. Sugiura: 1987, 'The Current – Voltage Relationship in Auroral Current Sheets'. *J. Geophys. Res.* **92**, 187.

Weimer, D. R., L. A. Reinleitner, J. R. Kan, L. Zhu, and S. I. Akasofu: 1990, 'Saturation of the auroral electrojet current and the polar cap potential'. *J. Geophys. Res.* **95**, 18981.

Winglee, R. M. and J. D. Menietti: 1998, 'Auroral activity associated with pressure pulses and substorms: A comparison between global fluid modeling and Viking UV imaging'. *J. Geophys. Res.* **103**, 9189.

Address for Offprints:
Dr. Joachim Raeder
Institute of Geophysics and Planetary Physics
University of California
Los Angeles, CA 90095-1567 USA
Phone: +310-267-2338
Fax: +310-206-3051
e-mail: jraeder@igpp.ucla.edu
Web: http://pallas.igpp.ucla.edu/jraeder